

Phonon scattering from residual defects in GaAs: Observation of optically induced metastability by phonon imaging

J. A. Shields* and J. P. Wolfe

Physics Department and Materials Research Laboratory, University of Illinois at Urbana-Champaign, Urbana, Illinois 61801

(Received 22 November 1993)

Phonon imaging with frequency-selective detectors is used to probe the scattering from residual defects in semi-insulating GaAs. As in previous heat-pulse studies, we find that the transmission of non-equilibrium phonons with longitudinal and transverse polarizations can be modified by near-infrared excitation of the crystal at low temperatures. These effects have been attributed to metastable states of the ubiquitous *EL2* defect in liquid-encapsulated-Czochralski-grown GaAs. In the present work we use the dispersive shifts in the phonon-focusing pattern to gain information about the frequency dependence of these optically induced changes. For particular polarizations and propagation directions, near-infrared excitation causes a huge decrease in the scattering of phonons with frequencies above 700 GHz. Our results show that, unlike the elastic scattering of simple mass defects, the residual defects are effective *inelastic* scatterers of phonons. An analysis of our data based on the theory of Nowick and Berry indicates that the change in the transmission of phonons following photoexcitation cannot be attributed to a unique symmetry change of a single defect.

I. INTRODUCTION

While the traditional methods of thermal conductivity yield useful mode-averaged phonon-scattering rates for a wide variety of solids, the nonequilibrium methods of ballistic heat pulses have the potential to uncover fine details of the phonon-scattering processes in selected materials. With the developments in phonon imaging and phonon spectroscopy, it is possible to isolate phonons of a given polarization, propagation direction, and frequency. Over the past several years quantitative methods have been introduced which measure the *elastic* scattering rates of high-frequency phonons in semiconducting (or insulating) crystals. By combining phonon-imaging with frequency-selective tunnel-junction detectors and a slotted-sample geometry, Shields *et al.*¹ were able to measure the intrinsic scattering from isotopic defects in high-purity Si. The results were in essential agreement with the basic theory of mass-defect scattering introduced in 1955 by Klemens² and computed with elastic anisotropy by Tamura.³

A subsequent study of undoped GaAs by Ramsbey, Tamura, and Wolfe⁴ found that scattering of acoustic phonons from intrinsic isotopes could explain the propagation of longitudinal phonons, but the transverse phonons displayed a scattering rate at least four times greater. This mode-selective scattering rate was attributed to inelastic scattering from residual defects in the semi-insulating GaAs, possibly associated with the ubiquitous *EL2* defect which acts to compensate crystals grown by the liquid-encapsulated-Czochralski (LEC) method. The present study is motivated by a desire to understand the nature of this extrinsic scattering. An overall aim is to find a systematic approach to understanding the phonon scattering from impurities and point defects in semiconductors.

Several previous studies have suggested the utility of heat-pulse methods to characterize defect symmetries in semiconductor crystals. Ground-breaking experiments by Narayanamurti, Chin, and Logan⁵ used heat pulses to determine the local symmetry of chromium impurities in semi-insulating GaAs. The phonons were produced by a thin-film Constantan heater deposited on one face of the crystal and detected on the opposite face by a thin-film superconducting Al bolometer. They compared the phonon transmission of the longitudinal (*L*), fast-transverse (FT), and slow-transverse (ST) modes along the three major symmetry directions for samples with different doping concentrations of Cr. Differential scattering of the three modes was observed for the samples doped with Cr at a concentration of about 10^{17} cm⁻³. Comparison of the mode- and direction-dependent scattering with the theory of anelastic wave scattering by Nowick and Berry⁶ led Narayanamurti, Chin, and Logan to conclude that Cr has a tetragonal site symmetry in their samples. Earlier electron spin resonance (ESR) data suggested a tetragonal site symmetry for Cr²⁺, but an orthorhombic site symmetry for Cr³⁺, implying that the dominant defect in Narayanamurti's experiments was Cr²⁺. These researchers extended their study to the *DX* center in films of Al_xGa_{1-x}As doped with Sn or Te donors and concluded that the Sn sites were trigonal and the Te sites were most likely orthorhombic.⁷ Related phonon-spectroscopy studies of Cr³⁺ in GaAs were conducted by Hamdache *et al.*⁸

Mode-dependent scattering of phonons from residual defects (presumed *EL2*) in GaAs has been observed by Culbertson, Strom, and Wolf.⁹ They employed the characteristic metastability of this defect to isolate its effect on the phonons. Basically, when the sample is irradiated with near-infrared radiation at low temperatures, the charge state of the defect is changed. Heating the

sample above about 140 K causes a recovery to the previous "normal state." Culbertson, Strom, and Wolf used a laser for phonon generation and a $0.5 \times 0.5 \text{ mm}^2$ NbN bolometer for detection. Time traces of the heat pulses were recorded for the three major symmetry directions with the *EL2* defect in the normal and metastable states. Comparison of the relative phonon intensities with the selection rules for anelastic relaxation led to the conclusion that the transition to the metastable state corresponds to a reduction in the number or scattering strength of trigonal scattering centers.

In this paper we bring to bear on this problem the high angular resolution of phonon imaging. By examining the phonon flux as a continuous function of propagation direction (not just along symmetry axes) and using frequency-selective detectors, we have found that the phonon scattering from residual defects in GaAs is more complex than suggested by the previous work. When a tunnel-junction detector (sensitive primarily to high-frequency phonons) is used, our sample of LEC-grown GaAs displays qualitatively similar mode selectives along symmetry axes as those observed by Culbertson, Strom, and Wolf. However, when a broadband Al-bolometer detector is used, very different results are obtained. Using the tunnel-junction detector, we observe striking changes in the phonon-focusing pattern when the crystal is irradiated, implying that the phonon absorption spectrum of the crystal is sensitive to the electronic states of the defects. In other words, the inelastic scattering of phonons (e.g., frequency down conversion) is highly sensitive to the types and states of the defects.

II. IMAGING EXPERIMENTS WITH FREQUENCY-SELECTIVE DETECTORS

Since one of the motivations of this study is to explain the mode-selective scattering rate in GaAs measured by Ramsbey, Tamura, and Wolfe, the same sample is used. It is an undoped GaAs crystal from Wacker Chemitronics,¹⁰ 1.94 mm thick with a 0.25-mm-thick slot parallel to the (110) faces (explained below). A 2000-Å-thick copper film was evaporated over the entire excitation surface to absorb the incident Ar^+ laser pulse as the heat source. As in the usual phonon-imaging experiments, the focused laser beam can be scanned across the face to produce "line scans" or complete images of heat flux, as detected by a fixed detector on the opposite face. All experiments are performed with the sample in superfluid helium at about 2 K.

The transition to the metastable state(s) of the defect(s) is accomplished by irradiating the sample with a Nd:YAG (where YAG denotes yttrium aluminum garnet) laser at a wavelength of $1.06 \mu\text{m}$ with an intensity of approximately 5 mW/cm^2 for 5 min. The $1.06\text{-}\mu\text{m}$ (1.17 eV) laser line is very close to the peak in the absorption which causes the transition to the metastable state associated with the *EL2* defect.¹¹ The recovery of the normal state is accomplished by warming the sample up to 140 K. The defocused YAG laser is incident from the detector side of the crystal, which is partially obscured by the contacts to the detector.

Our first detector is a superconducting PbBi tunnel junction with a sensitivity onset of about 700 GHz (the energy needed to break Cooper pairs). The characteristics of these phonon detectors are described in Ref. 12. The junction used in these experiments proved to have a significant sensitivity for lower-frequency phonons also. However, the large increase in sensitivity at 700 GHz provides much different results than in the Al-bolometer experiments described later. By virtue of its broadband sensitivity, the bolometer signals are dominated by the much more prevalent phonons with frequencies well below 700 GHz.

The phonon transmission along the three major symmetry axes is indicated by the heat pulses shown in Fig. 1. The heat pulses are characterized by sharp onsets at the ballistic times of flight of the *L* and *T* phonons and long tails corresponding to phonons which have scattered in the bulk of the crystal. The diffusive tails are more prevalent for the transverse phonons than for longitudinal, indicating a larger scattering rate for transverse phonons. The heat pulses are significantly modified after infrared radiation. Only the [110] case shows the relative intensities, before and just after radiation; the signals are normalized to the peak intensity in the other two cases. It is clear that the *L* and *T* phonons are differentially

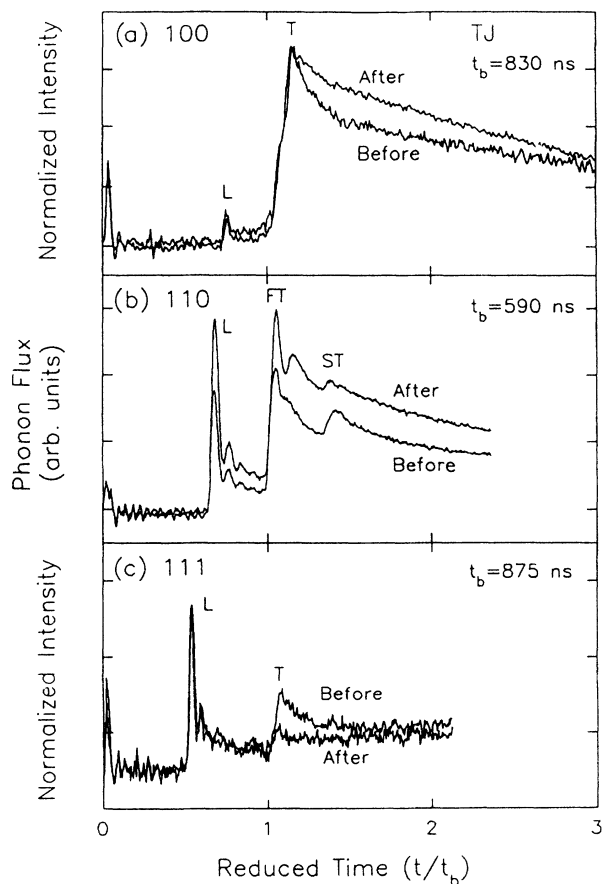


FIG. 1. Phonon time traces for the three major symmetry directions before and after Nd:YAG irradiation. The horizontal scale is the reduced time, t/t_b . Only (b) exhibits relative intensities: (a) and (c) have been normalized.

affected by the light, especially for [111] propagation, Fig. 1(c). The results will be tabulated later.

By using the slot in the sample, as illustrated in the inset of Fig. 2(b), we can isolate the optical effect on the scattered and ballistic phonons. With the laser at position *S*, only scattered phonons are detected, as the ballistic path is blocked by the slot. We see from Fig. 2(a) that the number of scattered phonons is increased after irradiation. By moving the laser spot to position *T*, we detect the scattered plus ballistic phonons as shown in Fig. 1(b). Subtracting the "scattered-only" signal of Fig. 2(a), we obtain the "ballistic-only" signal plotted in Fig. 2(b). As expected, the long tails are much reduced. Most importantly, we see that the ballistic signals are also increased after radiation.

This is a very important result. It says that the total number of high-frequency phonons detected by the tunnel junction—both ballistic and scattered—are increased after infrared irradiation. We conclude that the normal states of the defects more effectively down-convert phonons than the metastable states. This result implies an *inelastic* scattering process involving a change in the phonon frequencies. It is quite different from the scattering by mass defects in the crystal, which is known to be elastic. The reduction in inelastic scattering (and thus the reduction of frequency down conversion) results in a transmitted phonon distribution with a higher average

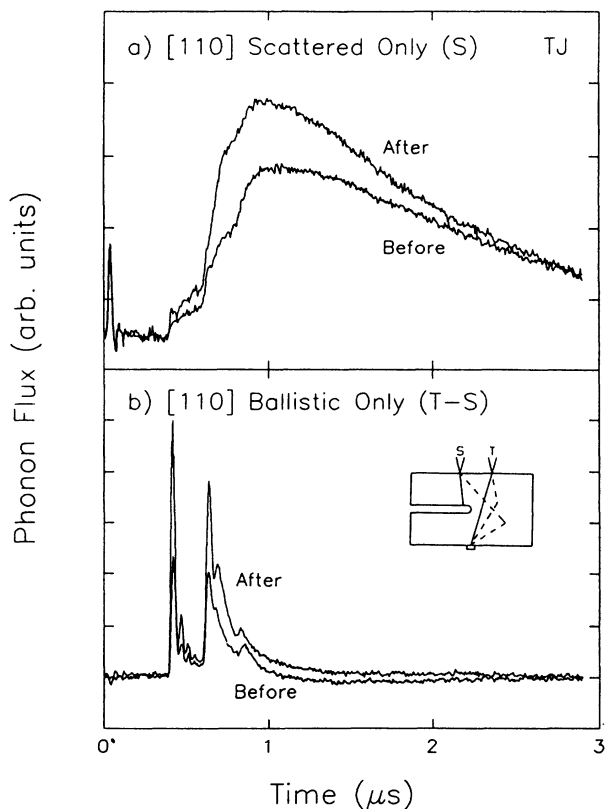


FIG. 2. Phonon time traces approximately along the [110] propagation direction for (a) the scattered-only flux and (b) the ballistic-only flux, before and after YAG irradiation, taken with the tunnel-junction detector.

frequency. Since the tunnel-junction frequency onset is 700 GHz, it is not very sensitive to the corresponding decrease in lower-frequency phonons.

A striking confirmation of this conclusion is provided by the phonon-imaging experiment shown in Fig. 3. Here we show phonon images obtained by raster scanning the laser beam and at each laser position recording the heat-pulse intensity integrated over a broad time gate.

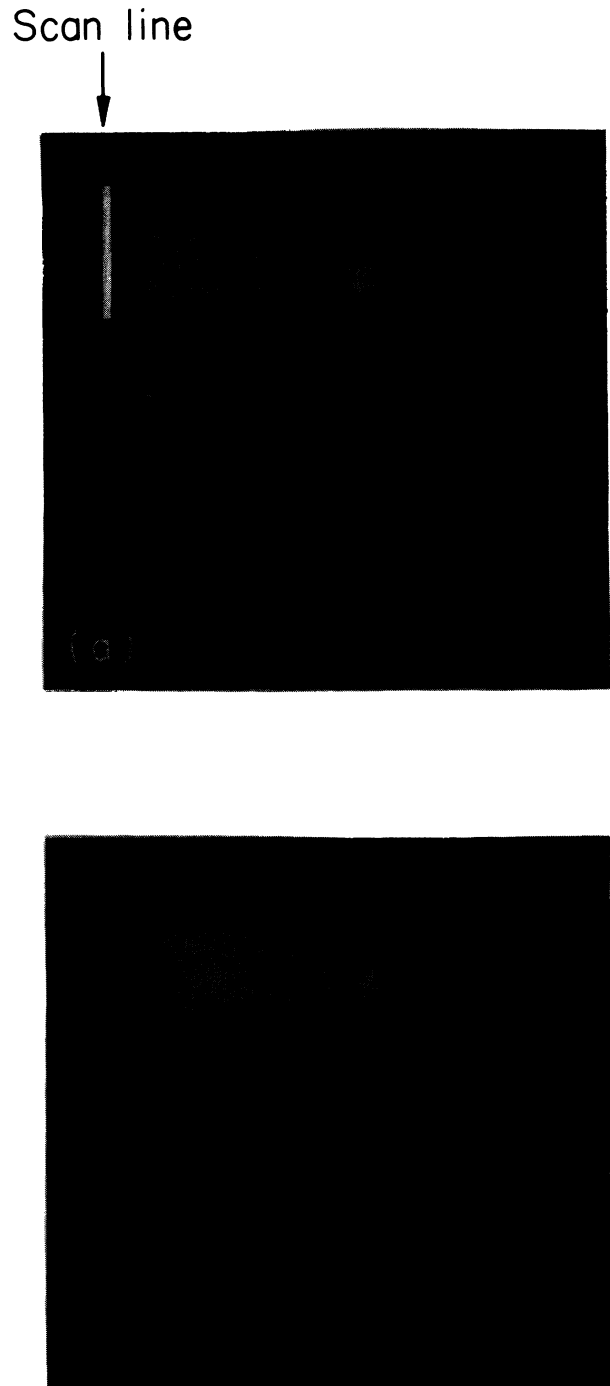


FIG. 3. Experimental phonon images of GaAs taken with a tunnel-junction detector (a) before and (b) after irradiation of the sample with the Nd:YAG laser.

The sharp features are the well-known phonon-focusing caustics, blocked by the slot at the far left. Before radiation [Fig. 3(a)], the caustic pattern is characteristic of ballistic phonons with frequencies of about 300 GHz and lower. After radiation [Fig. 3(b)], a new set of caustics appears, superimposed on the low-frequency pattern. The new caustics, shifted by phonon dispersion,¹² correspond to phonons with frequencies about 700 GHz—the principal sensitivity onset of the tunnel-junction detector. Similar caustic shifts have been observed in a number of crystals¹³ by systematically varying the detector frequency and are well explained by lattice dynamics models. Here the shift in the caustic pattern acts as a sort of phonon spectrometer to distinguish the transmission of phonons with different frequencies.

As seen from the phonon images, the low-frequency phonons are still present after irradiation, but the number of high-frequency ballistic phonons is greatly increased. And those with frequencies greater than 700 GHz are most effectively detected with this tunnel junction. A quantitative measure of this effect is given by a line scan across the FT-caustic ridge, as identified in Fig. 3(a) and plotted in Fig. 4(a). The low-frequency caustics (peaks) still remain after irradiation, but a much broader FT ridge is superimposed.

If we now set the laser at position *D* shown in Fig. 4(a)

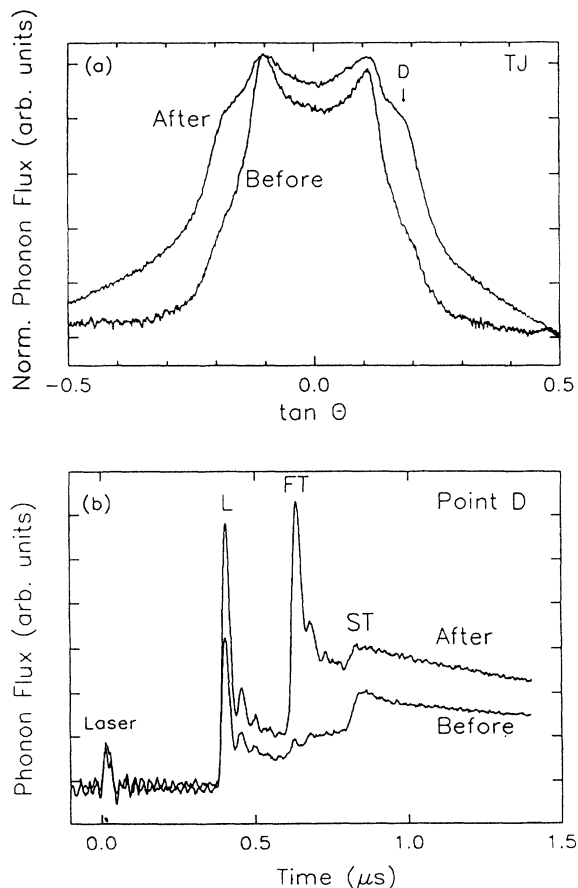


FIG. 4. (a) Line scans taken parallel to the slot boundary across the FT ridge before and after YAG irradiation. (See Fig. 3.) (b) Time traces taken at the point labeled *D* in (a), before and after YAG irradiation.

and look at the corresponding time traces for this propagation direction, a very striking result is found, as shown in Fig. 4(b). Before irradiation, the FT phonon signal is almost non-existent, as we are sampling the flux “off the ridge.” After irradiation, a huge FT signal arises, obviously from those FT phonons in the broader ridge. These are phonons which are almost completely scattered by the defects in the normal state. When the metastable state is induced, these high-frequency phonons pass much more freely through the crystal. We also see from Fig. 4(b) that the ST phonons react differently, actually decreasing after irradiation (ignoring the background of scattered FT phonons). Clearly, the scattering processes associated with the residual defects (presumably *EL2*) are highly polarization selective.

The experiments described above have been repeated using a granular aluminum bolometer to achieve broadband phonon detection. More of the sample was masked from the infrared radiation due to larger contacts, so quantitative comparisons with the tunnel-junction experiments is not possible. Qualitatively, however, we shall see marked differences. While the bolometer detects both high- and low-frequency phonons, the resulting heat pulses and images are dominated by the low-frequency phonons, which are in much greater abundance.

Figure 5 shows the time traces taken in the three major

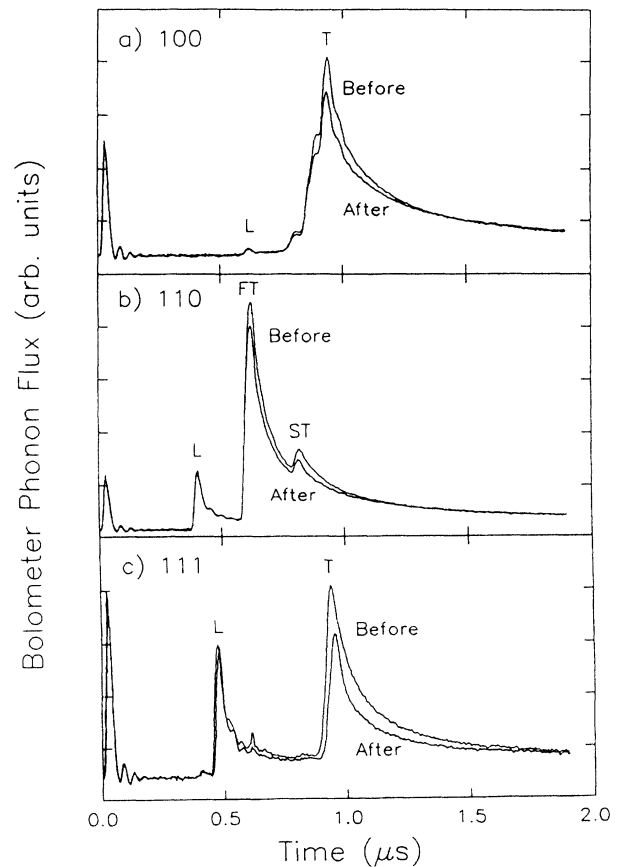


FIG. 5. Phonon time traces for the three major symmetry directions taken with a bolometer detector before and after YAG irradiation. The relative intensities for each propagation direction are recorded.

symmetry directions both before and after irradiation with the YAG laser. In each case, the "before" and "after" signals represent the relative changes in intensity. (The first pulse arriving at $t=0$ is produced by directing a small fraction of the Ar^+ laser beam onto the detector and is used to check the absolute sensitivity calibration.) The longitudinal intensities change very little with optical irradiation. The change along any of the symmetry directions is less than the measurement uncertainty of 10–20%.

In contrast to the tunnel-junction case, the ballistic signals from the transverse phonons all decrease with optical irradiation. By the method described above, we separate the scattered and ballistic signals and the results for [110] propagation are shown in Fig. 6. An apparent slight increase in the number of scattered phonons accompanies the obvious decrease in the number of ballistic phonons in the FT ridge. The tail accompanying the ballistic-only pulse may be due to the decay time of the localized heater source, which may be extended by the creation of a helium bubble at the excitation point.¹⁴

The phonon image obtained with the bolometer, Fig. 7(a), shows only the low-frequency caustic pattern, unchanged after irradiation. The changes in ballistic and scattered flux may be characterized by a spatial scan along the FT ridge, perpendicular to the slot boundary, as shown in Fig. 7(b). The signal from scattered phonons collected "behind the slot" is virtually unchanged by the optical excitation, whereas the FT ballistic signal de-

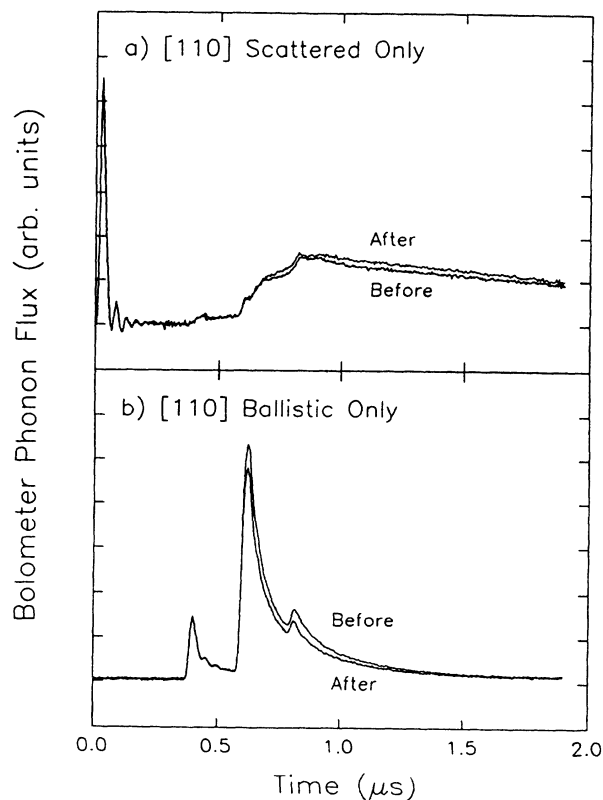


FIG. 6. Phonon time traces approximately along the [110] propagation direction for (a) scattered-only flux and (b) ballistic-only flux, taken with a bolometer detector before and after YAG irradiation.

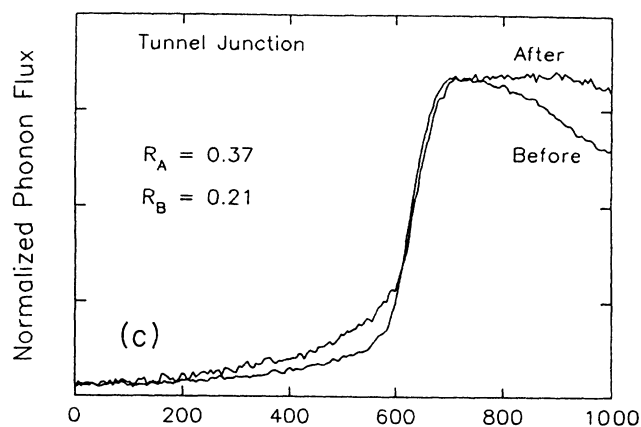
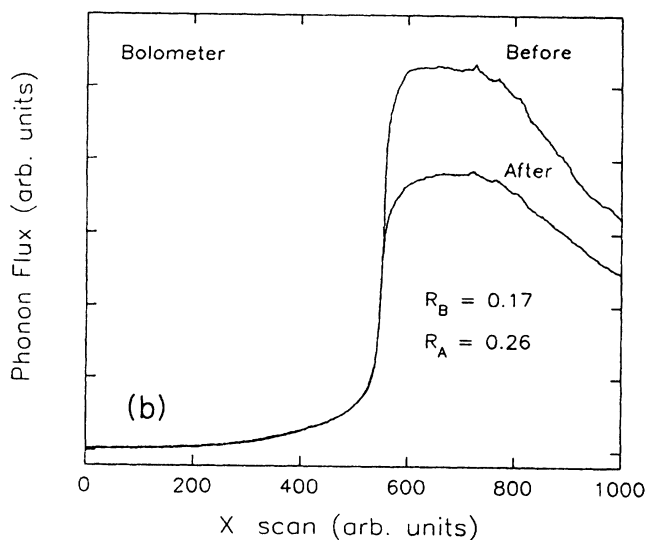
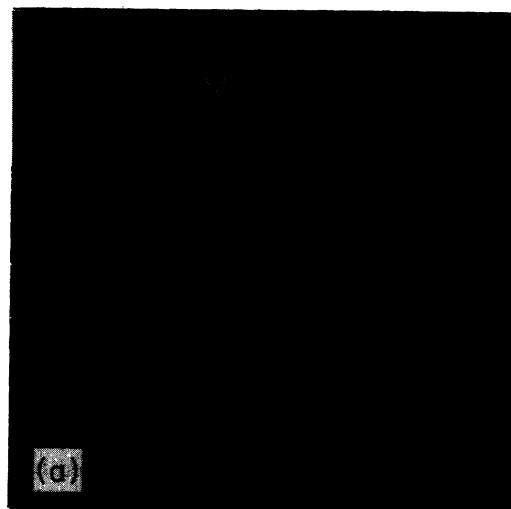


FIG. 7. (a) Experimental phonon image taken with a bolometer detector before irradiation with the YAG laser. (b) Line scans through the center of the FT ridge, perpendicular to the slot boundary before and after YAG irradiation. (c) Same with tunnel-junction detector.

TABLE I. Selection rules governing anelastic relaxation. An X indicates an interaction exists between that stress and a defect of that symmetry. C_{44} and $C' \equiv C_{11} - C_{12}$ are two of the three symmetrized stresses. The third symmetrized stress corresponds to the application of hydrostatic pressure and produces no phonon-defect interaction.

"Stress"	Defect symmetry		
	Tetragonal	Trigonal	Orthorhombic (100) (110)
C'	X		X X
C_{44}		X	X

creases significantly. The ledge ratio R is defined as the scattered signal just beyond the slot divided by the total (scattered plus ballistic) signal just before the ballistic path is blocked by the slot. The amount of decrease in ballistic component varies from experiment to experiment, ranging from 33% to 55% for the transverse phonons.¹⁵ Spatial scans across the slot were also taken for the tunnel-junction case, and an example is shown in Fig. 7(c). These data also displayed great variability from run to run, but always showed an increase in the scattered fraction (R) after irradiation. Apparently, the number of electrons in metastable states is sensitive to the irradiation or starting conditions.

The tunnel-junction data show an increase in the scattered component [ledge ratio in Fig. 7(c)] concurrent with the increase in the number of ballistic phonons above 700 GHz [Fig. 4(b)], implying that the metastable state produces less inelastic but more elastic scattering than the normal state. The decrease in the ballistic component of low-frequency transverse phonons after optical excitation (Fig. 5) is consistent with an increase in elastic scattering. The complexity of these results suggests that studies limited to a single sample will not resolve all the microscopic details; nevertheless, we briefly discuss the inelastic scattering of phonons from impurities in an attempt to provide a framework for understanding these and later experiments.

III. THEORETICAL CONSIDERATIONS

For defects with the same point symmetry as the atoms in the pure crystal (e.g., for isotopes, substitutional im-

TABLE II. Phonon velocities along the three major symmetry directions.

Direction of \mathbf{k}	$v_L^2 \rho$	$v_{FT}^2 \rho$	$v_{ST}^2 \rho$
[100]	$2C' + C''$	C_{44}	C_{44}
[110]	$(C' + 2C'' + 6C_{44})/6$	C_{44}	$C'/2$
[111]	$(C'' + 4C_{44})/3$	$(C' + C_{44})/3$	$(C' + C_{44})/3$

purities, vacancies, etc.) simple mass-defect scattering can be used to explain the scattering. The scattering rate is theoretically independent of the phonon mode and polarization. In studies of ultrasonic attenuation, it has been shown that for defects with symmetries lower than that of the crystal (e.g., interstitials, complex defects, or distorted substitutional impurities) *anharmonic* vibrations may occur which lead to frequency conversion of elastic waves. Termed "anelastic relaxation" in the basic formulation of Nowick and Berry,⁶ this type of process may be viewed as a nonequilibrium response of the crystal-defect system. In the present case, anelastic relaxation of the defect can produce anisotropic phonon scattering, i.e., the scattering rate depends on the direction and the polarization of the incident phonon.

The possibility that an elastic wave propagating along a given symmetry direction can interact with the defect may be determined from the selection rules governing anelastic relaxation.⁶ The symmetry-allowed couplings are shown in Table I for a cubic crystal. Here the phonon stress is labeled by the elastic constants which are involved. Given the L and T velocities tabulated in Table II, it is convenient to combine the three cubic elastic constants, C_{11} , C_{12} , and C_{44} , into the symmetrized combinations, $C_{44} = C_{44}$, $C' = C_{11} - C_{12}$, and $C'' = C_{11} + 2C_{12}$. The X's in Table I indicate that an interaction occurs and the blanks show the absence of an interaction. Given this information, we can determine how phonons with wave vectors along a given symmetry axis couple to defects of various symmetries. The results are tabulated in Table III, which includes the results given for transverse modes by Narayanamurti, Chin, and Logan.⁵ The X's indicate whether a phonon of given mode and wave-vector direction couples to a defect with a particular symmetry. This type of table is particularly useful for ultrasonic waves, where a planar transducer mounted on a symmetry face of the crystal produces a wave vector normal to that face.

TABLE III. Anelastic selection rules for various phonons. An X indicates the presence of an interaction between a phonon of that mode and direction with a defect of a certain symmetry.

Mode	Direction of \mathbf{k}	"Stress"	Defect symmetry			
			Tetragonal	Trigonal	Orthorhombic (100)	Orthorhombic (110)
T	[100]	C_{44}		X		X
FT	[110]	C_{44}		X		X
ST	[110]	C'	X		X	X
T	[111]	C_{44}, C'	X	X	X	X
L	[100]	C'	X		X	X
L	[110]	C_{44}, C'	X	X	X	X
L	[111]	C_{44}		X		X

Unfortunately, Table II does not contain sufficient information to adequately treat the propagation of ballistic heat pulses along arbitrary crystalline directions. Furthermore, even the phonon flux detected along a symmetry axis generally includes contributions from wave vectors not pointing along that axis. This is because the group-velocity surface has folded sections, implying that phonons with different wave vectors can propagate along the *same* real-space (group-velocity) direction.

To treat this problem properly, one must compute the coupling strength between a phonon of given mode and wave vector and the defect of a given symmetry. This process of calculating for a given phonon the “resolved shear stress” which couples to the defect has been accomplished for extended defects—dislocations in LiF. Northrop *et al.*¹⁶ produced a two-dimensional map of the interaction strength for each phonon mode. This map was then used as a transmission function, which is multiplied by the ballistic phonon distribution, to obtain a phonon image of ballistic flux in the presence of the defects. This procedure has not been applied to point defects so far, as it seems reasonable to choose a well-defined defect and crystal that are experimentally accessible. The *EL2* system, where the identification of the defect (or family of defects) is still up to question, is probably not the best place to test such a theory.

IV. DISCUSSION AND CONCLUSIONS

Cognizant of the limitations discussed above, we compare our data to the predictions of Table III, assuming that the ballistic heat pulses propagating along a symmetry axis contain phonons with wave vectors sufficiently close to that axis that the selection rules have some validity. The results are less than satisfying, perhaps due to a multiplicity of residual defects rather than the noncollinearity of wave vector and group velocity.

An additional factor in the present experiments is that the normal and metastable states of *EL2* probably have different symmetries. By optically inducing a change from the normal to the metastable state, we would expect to observe the *change* in symmetry between the two states not the symmetry of either one. The results of the pho-

non time traces along the symmetry directions for both the tunnel-junction data and the bolometer data are tabulated in Table IV. Both the sign and the magnitude of the intensity change following near-infrared excitation are given, as well as the variances over several runs. Some of the variation observed in the measurements may be due to a difference in illumination of the sample, since the electrical contacts covered a significant fraction of the illuminated surface. Table IV also includes a summary of the data of Culbertson, Strom, and Wolf,⁹ who used a NbN bolometer. It is interesting that their data qualitatively agree with our tunnel-junction data, suggesting that the NbN detector may have been more sensitive to the higher-frequency phonons. However, one cannot rule out differences in the two LEC-grown samples. After all, we are dealing with residual defects in the crystal.

We see that the transition from the normal to the metastable state is accompanied by a change in both the C_{44} and C' rows for the transverse modes (it is difficult to make conclusive statements concerning the longitudinal mode, as discussed above). The change in C_{44} and C' could be explained by several combinations from the table of selection rules. For instance a change from a defect of tetragonal symmetry to one with trigonal symmetry should produce a decrease in the scattering of a C' mode and an increase in the scattering of a C_{44} mode. If the direction of change of the phonon flux for the transverse modes is included in the comparison, the bolometer data (mainly sensitive to lower-frequency phonons) are only consistent with the cubic to orthorhombic transition, while the tunnel-junction data (mainly sensitive to higher-frequency phonons) are consistent only with a trigonal to tetragonal transition. We conclude that for our sample of semi-insulating GaAs the phonon scattering is not simply characterized by anelastic scattering from a single defect.

Nevertheless, we believe that the methods described here, together with Monte Carlo calculations incorporating elastic and inelastic scattering mechanisms, have the potential for uncovering microscopic details of the defects or impurities. The present work has discovered large changes in the inelastic scattering strength of the residual defects in semi-insulating GaAs as the state of the defects is altered by optical excitation. The remarkable optically induced “transparency” of high-frequency

TABLE IV. Summary of the optically induced changes in heat-pulse intensity. Our results for tunnel-junction (TJ) and bolometer detectors are listed, as well as those of Ref. 9.

Mode	Direction	Stress	TJ data	Bolometer data	Culbertson data
<i>T</i>	[100]	C_{44}		-(16±4)%	+19%
FT	[110]	C_{44}	+36%	-(17±11)%	+46%
ST	[110]	C'	-62%	-(25±6)%	
<i>T</i>	[111]	C_{44}, C'		-(22±5)%	+17%
<i>L</i>	[100]	C'		<20%	
<i>L</i>	[110]	C_{44}, C'	+54%	<10%	+9%
<i>L</i>	[111]	C_{44}		<10%	+21%

FT phonons (Figs. 3 and 4) underscores the frequency and polarization sensitivities of the scattering from defects. To make further progress, a systematic case study is needed to isolate the effects of a single type of defect on the inelastic and elastic scattering of phonons before these methods can be applied to unknown defects.

ACKNOWLEDGMENTS

We acknowledge helpful discussions with Madeleine Msall. This work was supported in part by the National Science Foundation under the Materials Research Laboratory Grant No. DMR 89-20538.

*Present address: Advanced Micro Devices, P.O. Box 3453, 901 Thompson Place, Sunnyvale, CA 94088-3453.

- ¹J. A. Shields, S. Tamura, and J. P. Wolfe, *Phys. Rev. B* **43**, 4966 (1991); S. Tamura, J. A. Shields, and J. P. Wolfe, *ibid.* **44**, 3001 (1991).
- ²P. G. Klemens, *Proc. Phys. Soc. London, Sect. A* **68**, 1113 (1955).
- ³S. Tamura, *Phys. Rev. B* **30**, 849 (1984).
- ⁴M. T. Ramsbey, S. Tamura, and J. P. Wolfe, *Phys. Rev. B* **46**, 1358 (1992).
- ⁵V. Narayanamurti, M. A. Chin, and R. A. Logan, *Appl. Phys. Lett.* **33**, 481 (1978).
- ⁶A. S. Nowick and B. S. Berry, *Anelastic Relaxation in Crystal-line Solids* (Academic, New York, 1972).
- ⁷V. Narayanamurti, R. A. Logan, and M. A. Chin, *Phys. Rev. Lett.* **43**, 1536 (1979).
- ⁸M. Hamdache, P. J. King, D. T. Murphy, and V. W. Rampton, *J. Phys. C* **15**, 5559 (1982).
- ⁹J. C. Culbertson, U. Strom, and S. A. Wolf, *Phys. Rev. B* **36**, 2962 (1987).
- ¹⁰This undoped GaAs sample is originally from Wacker Electronics and was given to us by R. G. Ulbrich. The sample was polished with an alumina suspension and finally mechanically and chemically polished with SYTON™ colloidal silica.
- ¹¹G. M. Martin and S. Makram-Ebeid, in *Deep Centers in Semi-Conductors*, edited by S. T. Pantelides (Gordon and Breach, New York, 1986), Chap. 6; M. Kaminska, M. Skowronski, J. Lagowski, J. M. Parsey, and H. C. Gatos, *Appl. Phys. Lett.* **43**, 302 (1983).
- ¹²S. E. Hebboul and J. P. Wolfe, *Z. Phys. B* **73**, 437 (1989); **74**, 35 (1989).
- ¹³J. P. Wolfe, in *Festkörperprobleme (Advances in Solid State Physics)*, edited by U. Rössler (Vieweg, Braunschweig, 1989), Vol. 29, p. 75.
- ¹⁴J. A. Shields, M. E. Msall, M. S. Carroll, and J. P. Wolfe, *Phys. Rev. B* **47**, 12 510 (1993).
- ¹⁵J. A. Shields, Ph.D. thesis, University of Illinois at Urbana-Champaign, 1992.
- ¹⁶G. A. Northrop, E. J. Cotts, A. C. Anderson, and J. P. Wolfe, *Phys. Rev. B* **27**, 6395 (1983).

Scan line

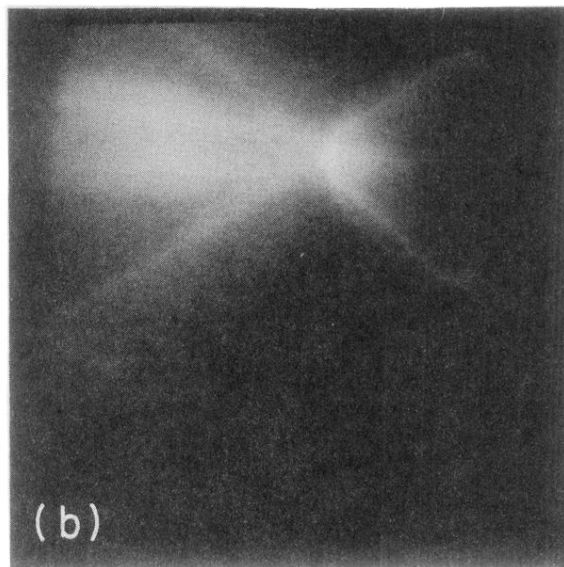
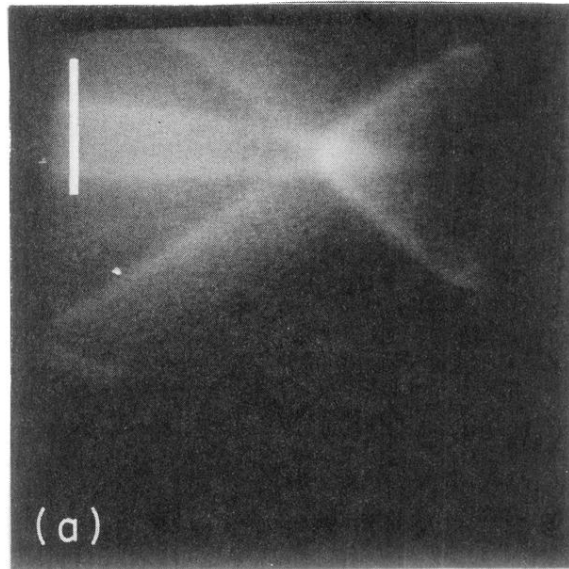


FIG. 3. Experimental phonon images of GaAs taken with a tunnel-junction detector (a) before and (b) after irradiation of the sample with the Nd:YAG laser.

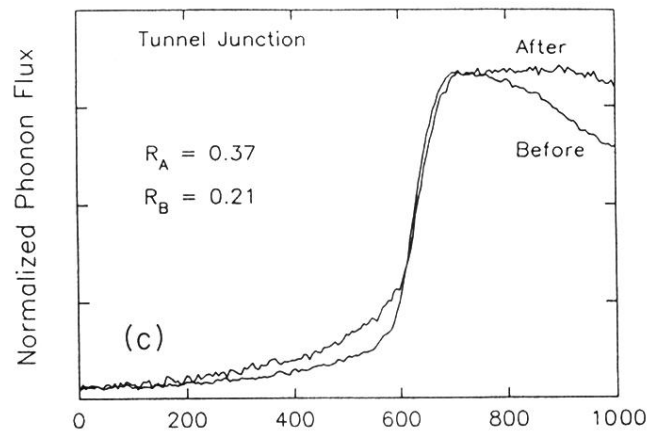
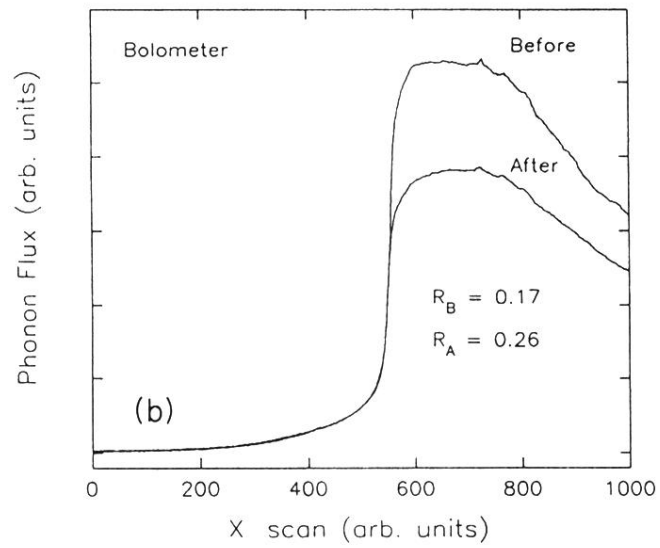
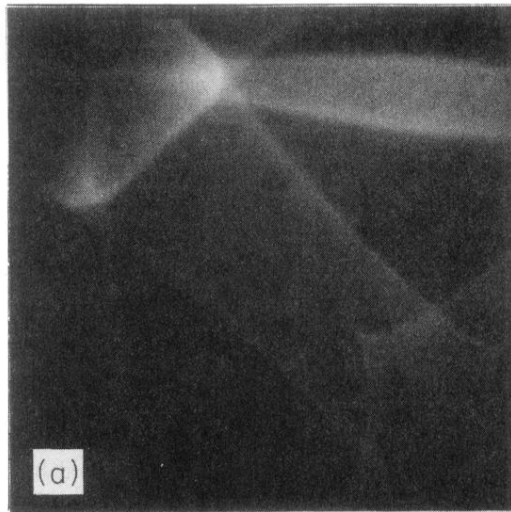


FIG. 7. (a) Experimental phonon image taken with a bolometer detector before irradiation with the YAG laser. (b) Line scans through the center of the FT ridge, perpendicular to the slot boundary before and after YAG irradiation. (c) Same with tunnel-junction detector.